

Unified Capacity Results for Free-Space Optical Communication Systems Over Gamma-Gamma Atmospheric Turbulence Channels

Himani Verma*, and Kamal Singh*

Abstract—Transmit power control, as in the mobile wireless channels, can enable a robust and spectrally efficient communication through atmospheric turbulence in terrestrial free-space optical (FSO) channels. With optical bandwidths in excess of several GHz and eye safety regulations limiting the transmit optical power, the per hertz signal-to-noise ratio (SNR) in terrestrial FSO systems can possibly become limited. This is especially true for future high-bandwidth and long-haul terrestrial systems based on coherent optical communications. Hence, power control becomes significant in terrestrial FSO communication systems. However, a comprehensive study of dynamic power adaptation in the existing FSO systems is lacking in the literature. In this paper, we investigate perfectly beam power-controlled terrestrial FSO communication systems with heterodyne detection and direct detection based receivers operating under shot noise-limited conditions. Under these systems considerations, we derive unified exact and asymptotic capacity formulas for the Gamma-Gamma turbulence channels with and without pointing errors. The numerical results highlight the intricate relations of atmospheric turbulence and pointing error parameters in typical terrestrial FSO channel settings. More importantly, a concrete assessment of the impact of the key channel parameters on the capacity performances of the aforementioned FSO systems is performed revealing several novel and interesting insights.

Index Terms—Optical beam power control, ergodic capacity, Gamma-Gamma atmospheric turbulence, heterodyne and direct detection, shot noise-limited conditions.

I. INTRODUCTION

Laser-based *free-space optical (FSO) communication* has emerged as an appealing alternative to RF (radio-frequency) and fiber technologies in providing efficient backhaul connectivity in the outdoor wireless networks. The key factors motivating this development are vast unregulated bandwidth, easy installation, inherent security, low-cost transceivers, etc [1]. In fact, interest in the applications of FSO-based wireless technologies has rapidly grown in recent years to design communications for diverse scenarios such as ad hoc wireless networks for tactical and disaster scenarios [1], terrestrial last-mile broadband access [2], deep-space exploration [3], inter-satellite links [4], civil and military applications [5], and the picture is still evolving for 5G and 6G wireless networks.

Most practical FSO communication systems currently in use employ either of the following two detection schemes:

(i) Intensity modulation with direct detection (IM-DD): In intensity-modulated optical systems, the information signal is conveyed by the intensity of the transmitted laser beam,

and there is effectively only *one degree of freedom*. At the receiver, the information is detected by direct impingement of the lightwave signal onto the front-end photodetector. Most commercially deployed FSO systems are based on IM-DD due to their simpler and low-cost transceiver design. However, the IM-DD scheme suffers from poor receiver sensitivity which, in turn, limits its usage to short-haul terrestrial links [6], [7]. **(ii) Coherent heterodyne detection (HD):** In coherent optical systems, information can be conveyed by simultaneous modulation of the optical carrier's amplitude and phase components, thus having potential for *two degrees of freedom*. Basically, coherent detection refers to the addition of a local optical signal (typically of different wavelength and hence the term 'heterodyne') to the incoming light beam before it impinges onto the photodetector. Compared with the direct detection scheme, the coherent detection scheme has an improved receiver sensitivity which can be traded off with the deployment distance (long-haul) if desired. Additionally, the coherent receiver can select a desired channel (in the electrical domain) using sharp RF filters (tuned at an intermediate frequency (IF), usually in the GHz range) and thus offers good selectivity. In contrast, the direct detection receiver selects a desired incoming lightwave signal using optical filters (typically wideband) and thus suffers severely from poor selectivity. For a detailed review of coherent detection-based optical receivers, see [7].

From the deployment perspective, FSO communication systems face two main practical challenges in terrestrial scenarios despite their appealing virtues: first, FSO communication is susceptible to the atmospheric turbulence-induced irradiance fluctuations¹ over a faster time-scale, and to the attenuation effects of absorption and scattering on a much slower time-scale [9]. This typically leads to poor performance and in some cases imposes unrealistic link budget requirements [10]. Second, since FSO communication is essentially *line-of-sight* (LOS) that rely on the highly directional beams and photodetectors, the optical link between the transmitter (Tx) and the receiver (Rx) is prone to pointing errors caused by dynamic wind loads, Tx-Rx motion/vibration, thermal expansion, building sway, etc. Both these factors, in unison or individually, are capable of degrading the performance of an FSO communication system drastically. The reader may refer to [10] for a comprehensive understanding of these

This work has been submitted to the IEEE for possible publication. Copyright may be transferred without notice, after which this version may no longer be accessible.

*The authors are with the Department of Electrical Engineering, Shiv Nadar Institution of Eminence, Delhi NCR, 201314, India (e-mail: hv790@snu.edu.in; kamal.singh@snu.edu.in).

¹Turbulence-induced irradiance fluctuation is a consequence of the atmosphere's refractive index fluctuation along the propagation path caused by the transverse component of the atmospheric wind movement, which in turn is generated due to random temporal temperature variations between the Earth's surface and the atmosphere. This small-scale turbulence effect is quite prominent for medium-to-long distance terrestrial FSO links [8].

fundamental issues and resulting performance limitations of the existing FSO systems for terrestrial applications.

In the optical wavelength regime (e.g., 850 nm/1550 nm), a laser beam transmitted on a terrestrial FSO link undergoes absorption, scattering, and irradiance fluctuations. Absorption and scattering are sensitive to atmospheric conditions such as rain, fog, and other obscurants, and the resulting optical wave attenuation is fairly deterministic. Turbulence, defined as random variations in the atmospheric refractive index, on the other hand induces wavefront distortion in the optical wave which in turn randomizes energy distribution within a cross-section of the beam leading to small-scale irradiance fluctuations [9], [11]. In the literature, several statistical models have been proposed for the irradiance fluctuation that have a strong basis in real FSO propagation scenarios. We mention a select few important and relevant models as follows: scintillation in weak turbulence is well modeled using log-normal distribution [12], [13], while the scintillation statistic in the weak-to-strong turbulence regimes is best described by Gamma-Gamma (GG) distribution [13]. In addition to the advantage of mathematical tractability, these scintillation models show excellent statistical fit with the simulation/experimental measurements [13]. Adjacently, the statistical modeling of the pointing error (jitter only) effect in the received irradiance has been carried out in [14] while the pointing error case with non-zero boresight is reasonably modeled in [15]. More recently, generalized turbulence models have been proposed based on Málaga (\mathcal{M}) distribution [16], double-generalized Gamma distribution [17], Fisher-Snedecor \mathcal{F} distribution [18], etc.

Transmit optical power in terrestrial FSO communications is limited due to stringent eye and skin safety regulations. Equally important, these FSO systems are designed to exploit virtually unlimited and unregulated bandwidth (several GHz of optical bandwidth in practice) [10]. Based on these facts, it is not hard to show that the available transmit power per hertz can be limited in practice irrespective of the total amount of available transmit optical power. The turbulence-induced irradiance fluctuations (mentioned earlier) present in the terrestrial FSO channels further degrade the power collected at the receiver side [9], but this degradation can be alleviated through power control. Hence power control at the FSO transmitters becomes practically important, especially for future high-bandwidth and long-haul terrestrial applications. Moreover, power control at the optical laser transmitters can also prolong the life span of the laser sources [10]. With the FSO transmitter capable of tracking the optical channel variations, the power of the optical laser beam can be adapted according to the channel conditions. Consider, for example, a naive scheme where the laser source transmits only when the instantaneous channel is good (above a threshold) which might be reasonable at a low-power budget. The *main objective* of the paper is to present a unified treatment of terrestrial FSO communication systems with direct detection (DD) and heterodyne detection (HD) receivers with an emphasis on spectral efficiency improvement: dynamic power adaptation at the laser beam source to exploit the temporal irradiance fluctuations created by the atmospheric turbulence and/or pointing error conditions. Our results provide several novel insights into the

scintillation effects of turbulence and pointing error on the capacity losses/gains in these terrestrial FSO systems.

Several studies have analyzed the capacity performance of terrestrial FSO systems based on IM-DD and HD detection schemes operating over Gamma-Gamma and Log-normal turbulence conditions (see [19], [20], [21], [22] and references cited therein), and more recently over generalized turbulence channels (see [23], [24], [25], [26] and references cited therein), etc. However, almost all of these research works have not considered the crucial power control aspect at the optical transmitters for terrestrial FSO links. This is largely due to the analytical difficulties in solving the optimization problems involved (and also capacity integrals in some cases). In [27], [28], Lapidoth and Moser provide capacity bounds for the (unfaded) IM-DD based FSO channel under average and/or peak power constraints imposed on the intensity of the laser beam. In particular, it is shown that the capacity bounds (both upper and lower) under average-power constraint converge to the same limit at high optical powers [27, Theorem 7 and Proposition 8], which we will utilize later (in subsection III-C) to develop the capacity utility for the input-dependent IM-DD FSO system model.

A. Contribution and Organization of This Paper

In this paper, we focus on FSO communication through the atmospheric turbulence with the possibility of lack of perfect alignment of the transmitter and receiver. Section II presents the details of the GG atmospheric turbulence and the pointing error model adopted in this work. The considered FSO system models and the relevant noise sources are described in detail in Section III. We list the key contributions of this paper below with respect to closely related earlier works:

- With the motivation for the dynamic beam power control in terrestrial FSO systems firmly established, we present ‘exact’ closed-form solution (unified for both IM-DD and HD schemes) in Section IV for the ergodic capacity of the Gamma-Gamma turbulence channel with optical beam power control allowed at the FSO transmitter (with perfect channel knowledge). Theorems 6 and 7 are our main results derived for the turbulent channel capacity with and without pointing error: a unified integral-form capacity expression is created (for both IM-DD and HD schemes) which is then solved meticulously in closed-form (the details of the derivation in Section V); a key role is played by the identity in Lemma 17 which is new to the best of our knowledge. This solution is further simplified in the asymptotic regimes of optical powers (Theorems 8 and 9) providing novel and interesting insights into how the performance of existing FSO systems depend on the basic turbulence and pointing error parameters in action. To focus more on the implications of these results, the proofs of the exact and asymptotic results are relegated to Sections V and VI respectively.
- A particular concern in the numerical results presented in the existing FSO works [19], [20], [21], [23] and [24] (mentioned earlier) is the lack of clarity on how a wide range of atmospheric turbulence is realized. Some of the FSO channel parameters are intertwined: varying the FSO link-length alters the turbulence statistics (and path loss) as

well as the pointing jitter statistics if present. It is critical to understand the channel parameters (and the underlying physics) for the chosen atmospheric turbulence profiles. If neglected, this may lead to inaccurate results and flawed insights in the worst case. We first highlight this concern in subsection IV-C and justify the FSO systems and turbulence channel settings used for the numerical results. Several concrete and novel insights are derived in subsection IV-C, for example: i) at high SNRs, the capacity of the optical channel with pointing errors improves with turbulence (see Fig. 3), and ii) the capacity improves with atmospheric turbulence at sufficiently low SNRs (see Fig. 9). These interesting capacity penalties/improvements are also further characterized and justified in detail.

- As per the authors' best knowledge, this is a first attempt at unified exact capacity analysis with *transmit beam power control* of IM-DD and HD schemes based FSO communication systems through GG atmospheric turbulence under shot noise-limited conditions. In contrast, a related recent work [24] focused on developing unified capacity results for the IM-DD and HD schemes under Málaga (\mathcal{M}) distribution (of which GG distribution is a special case) but for the case of constant beam power allocation (or no power control). In [19], an explicit solution is provided for the capacity of the IM-DD based FSO system over GG turbulence channels (with beam power control) with the receiver operating in thermal noise-limited condition; however, the crucial non-negativity condition at the IM-DD transmitter is omitted and thus, the results reported in [19] are inaccurate.
- While the IM-DD based FSO scheme is the simplest (in hardware) and widely used, this analytical study confirms that the HD based FSO systems are far superior in delivering high throughputs albeit with a more complex engineering design. The unified results presented in this work should assist the FSO system designer create a tradeoff between the two system choices under the cost and performance constraints. One step further, these results will serve as a baseline performance for future adaptive terrestrial FSO communication systems with strong practical constraints.

Finally, we review our main results and offer some concluding remarks in Section VII.

B. Mathematical Notations

We use the following notations throughout the paper: the probability density function (PDF) of a random variable X is denoted by $f_X(\cdot)$ and $\mathbb{E}[\cdot]$ denotes the expected value of the enclosed. The real, non-negative real and complex number sets are denoted by \mathbb{R} , \mathbb{R}^+ and \mathbb{C} , respectively. $\Gamma(\cdot)$ is the Gamma function [29, Eq. (8.310.1)], $K_\nu(\cdot)$ is the modified Bessel function of the second kind and order ν [29, Eq. (8.494.1)], $G_{p,q}^{m,n}(\cdot)$ is the Meijer-G function [29, Eq. (9.301)], $\psi(\cdot)$ is the Digamma function [29, Eq. (8.360.1)], and $\text{erf}(\cdot)$ denotes the standard error function [29, Eq. (8.250.1)]. All logarithms in this paper are natural logarithms.

II. OPTICAL FADING CHANNEL

The (overall) intensity fluctuation, also known as fading in the FSO literature, I of a transmitted laser beam due to

atmospheric turbulence and pointing error is modeled as

$$I = I_l I_a I_p \quad (1)$$

where I_l is the path loss component determined by the exponential Beers-Lambert Law for a given link length and weather conditions [30], I_a is the turbulence-induced scintillation, and I_p is the pointing-error induced fluctuation.

In this work, we consider that the large-scale component I_l is deterministic and fixed under the assumption of a fixed-length optical link with homogeneous weather conditions at all times. We will consider $I_l = 1$ for simplicity and instead focus on the small-scale components I_a and I_p which are independent and randomly time-varying in nature. In the following subsections, we describe the statistical models adopted for these fading constituents. These models are quite reasonable for medium to long-distance terrestrial FSO links.

A. Gamma-Gamma Atmospheric Turbulence

To cover a wide range of atmospheric turbulence from the weak-to-strong regime, the statistics of the intensity fluctuation I_a is well modeled using the Gamma-Gamma (GG) distribution as follows:

$$f_{I_a}(I_a) = \frac{2(ab)^{(a+b)/2}}{\Gamma(a)\Gamma(b)} I_a^{(a+b)/2-1} K_{a-b}(2\sqrt{ab}I_a); \quad I_a > 0 \quad (2)$$

where a and b are the distribution's shape parameters [13]. Ideally, the light from a laser source is understood to have a Gaussian beam profile, with its intensity distribution being a circularly symmetric Gaussian function across the beam cross-section and centered about the beam axis [31, Ch. 3]. Close to its center, the Gaussian beam is approximated by a plane wave, while the wave resembles a spherical wave when it is far from the beam waist yet inside the beam waist radius [31]. Considering optical radiation at the (far away) receiver to be a plane wave, the GG distribution parameters a and b can be directly related to atmospheric conditions through the following expressions [13]:

$$a = \left(\exp \left[\frac{0.49\sigma_R^2}{(1 + 1.11\sigma_R^{12/5})^{7/6}} \right] - 1 \right)^{-1}, \quad (3)$$

$$b = \left(\exp \left[\frac{0.51\sigma_R^2}{(1 + 0.69\sigma_R^{12/5})^{5/6}} \right] - 1 \right)^{-1}. \quad (4)$$

In this respect, $\sigma_R^2 = 1.23 C_n^2 k_w^{7/6} L^{11/6}$ denotes the Rytov variance determining the strength of the atmospheric turbulence, $k_w = 2\pi/\lambda_w$ is the optical wave number, where λ_w is the wavelength, L is the propagation distance, and C_n^2 is the index of refraction structure parameter. C_n^2 can be practically assumed to be constant for the line-of-sight propagation on horizontal paths [32].

B. Pointing Error

Pointing error is basically a mispointing of the laser beam with respect to the optical receiver that arises from i) boresight and ii) jitter: boresight is the *fixed* displacement between the received

beam centroid and the detection receiver center, whereas jitter is the *random* temporal displacement originating due to building sway, wind motion, Tx/Rx vibrations, etc.

In this work, we consider FSO communication between *fixed platforms* in terrestrial environments where it is reasonable to assume that the boresight problem can be made negligible by either careful system deployment or using a fast-tracking transmitter whereas the random jitter issue persists [9]. A Gaussian beam is typically defined in terms of its physical attributes such as intensity, beam divergence, beam waist, etc. Specifically, the waist w_L of a Gaussian beam is determined from the radial distance away from the axis where the irradiance drops to $1/e^2$ of the maximum intensity [31]. The transmitted laser beam, upon propagating a distance L , is incident on the receiving photodetector with an aperture radius r_A . The attenuation of the received optical beam due to turbulence-induced beam spread with pointing error (the misalignment is described by radial displacement r in the receiver plane between the centers of the beam footprint and the detector aperture) is given by $I_p(r; L) \approx A_0 \exp(-2r^2/w_{L_{\text{eq}}}^2)$ where $w_{L_{\text{eq}}}^2 = w_L^2 \sqrt{\pi} \operatorname{erf}(v) / (2v \exp(-v^2))$ is the (squared) equivalent beam width with $v = \sqrt{\pi} r_A / \sqrt{2} w_L$, and

$$A_0 = [\operatorname{erf}(v)]^2 \quad (5)$$

is the fraction of the collected power at $r = 0$ (i.e., no pointing error but only geometrical loss) [33]. Note that $0 \leq A_0 \leq 1$. For a coherent collimated beam, the beam radius w_L at the distance L is related to the beam waist w_0 at the exit aperture of the optical transmitter by $w_L = w_0(1 + \epsilon(\lambda_w L / \pi w_0^2))^{1/2}$ where $\epsilon = (1 + 2w_0^2/\rho_0^2(L))$ is the global coherence parameter and $\rho_0(L) = (1.46C_n^2 k_w^2 L)^{-3/5}$ is the coherence length of a plane wave propagating in turbulence [34]. Farid and Hranilovic [33] derived the PDF of the irradiance component I_p under the i.i.d. zero-mean Gaussian distribution assumptions for both the horizontal and vertical sways at the receiver (i.e., zero boresight and identical jitters) and is given by

$$f_{I_p}(I_p) = \frac{\xi^2}{A_0 \xi^2} I_p^{\xi^2-1}; \quad 0 \leq I_p \leq A_0 \quad (6)$$

where the parameter $\xi \triangleq w_{L_{\text{eq}}}/2\sigma_e$ is the ratio of the received equivalent beam waist $w_{L_{\text{eq}}}$ and the standard deviation of the pointing error displacement (jitter) at the detection receiver. It is important to keep in mind that the probability model (6) for pointing error is reasonable when $w_L/r_A \gg 1$ (see [33], [35]) and further that the effects of ξ and A_0 parameters are independent.

C. Gamma-Gamma Turbulence with Pointing Error

The PDF of the instantaneous composite irradiance I in terms of the independent constituents, namely the atmospheric turbulence I_a and the pointing error I_p , is obtained as follows:

$$f_I(I) = \int f_{I|I_a}(I|I_a) f_{I_a}(I_a) dI_a \quad (7)$$

where, $f_{I|I_a}(I|I_a)$ is the conditional PDF given I_a , and is expressed as

$$f_{I|I_a}(I|I_a) = \frac{\xi^2}{A_0 \xi^2 I_a} \left(\frac{I}{I_a} \right)^{\xi^2-1}; \quad 0 \leq I \leq A_0 I_a. \quad (8)$$

Substituting (8) and (2) in (7), we get

$$f_I(I) = \frac{2\xi^2(ab)^{(a+b)/2}}{(A_0 I)^{\xi^2} \Gamma(a)\Gamma(b)} I^{\xi^2-1} \cdot \int_{I/A_0}^{\infty} I_a^{(a+b/2)-1-\xi^2} K_{a-b} \left(2\sqrt{abI_a} \right) dI_a. \quad (9)$$

Recall that $I_l = 1$. A closed-form to the integral in (9) is provided by using the integral identity [29, Eq. (6.592.4)] with [29, Eq. (9.31.5)] as follows:

$$f_I(I) = \frac{ab\xi^2}{A_0 \Gamma(a)\Gamma(b)} G_{1,3}^{3,0} \left(\frac{abI}{A_0} \middle| \xi^2 - 1, a - 1, b - 1 \right). \quad (10)$$

Remark 1. $\mathbb{E}[I_a] = 1$ for the GG distribution in (2) and $\mathbb{E}[I_p] = A_0 \xi^2 / (1 + \xi^2)$ for the pointing error PDF in (6). Hence, the mean of the overall irradiance I is given by

$$\mathbb{E}[I] = \mathbb{E}[I_a] \mathbb{E}[I_p] = \frac{A_0 \xi^2}{1 + \xi^2}.$$

Remark 2. It should be noted that for $A_0 \rightarrow 1$ and $\xi \rightarrow \infty$, the composite irradiance distribution in (10) tends to the pure GG distribution in (2) as a special (extreme) case.

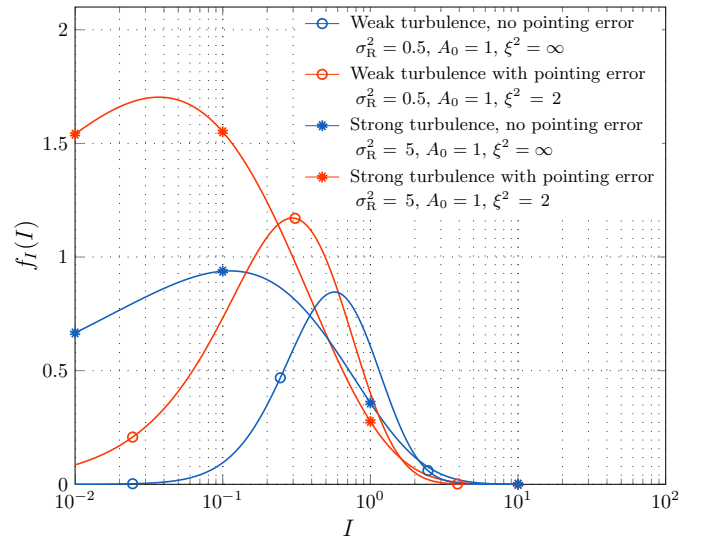


Fig. 1: The PDF of overall irradiance I in the weak and strong turbulence regimes. Higher atmospheric turbulence suggests an increased probability for small channel gains. The presence of pointing error also leads to probability concentration at low channel gains. These effects are enhanced in the figure for visual inspection by displaying intensity values on a log scale.

The overall irradiance distribution (10) is plotted in Fig. 1 for varying levels of turbulence and pointing errors. From this figure, we can notice that although turbulence-induced fading is the principal impediment, the sensitivity of the overall irradiance distribution to pointing error also becomes particularly acute even for mild random jitter variance. A more in-depth and unified understanding of the resulting performance loss in terms of channel capacity is an important objective of this paper.

III. SYSTEM MODELS & CAPACITY DEFINITION

We first provide a brief necessary background on the noise sources relevant to the FSO optical receivers in subsection III-A. We then proceed to develop the signal models for the *shot noise-limited* IM/DD and HD-based receivers in subsection III-B.

A. Receiver Noises in FSO Wireless Systems

In optical receivers, photodiodes are the most commonly used device to detect photons (or photodetection) with the objective of transforming an information-bearing optical signal into a photocurrent (electrical) signal with a one-to-one correspondence. Two fundamental sources of noise unavoidably stem out in the process of photodetection: i) the shot noise² arising due to photodetection itself, and ii) the thermal noise originating *post-detection* in the receiver circuitry.

Remark 3. *The electrical-to-optical (E/O) conversion at the transmit side and optical-to-electrical (O/E) conversion at the receiver typically admit losses which we have ignored for simplicity. These Tx./Rx. conversion losses can be adjusted in the optical link budget similar to the path loss component.*

The shot noise induced at the photodetector output is *signal-dependent* in the sense that its power grows linearly with the total incident optical power (say P_{in}). Since both thermal noise and shot noise are additive in nature and are statistically independent of each other, the total (electrical) noise variance can be expressed as their summation, i.e., $\sigma_{\text{Total}}^2 = \sigma_{\text{Th}}^2 + \sigma_{\text{Sh}}^2$, where $\sigma_{\text{Th}}^2 = \frac{4kT\Delta f}{R_L}$ and $\sigma_{\text{Sh}}^2 = 2qRP_{\text{in}}\Delta f$ denote the variance of thermal noise and shot noise, respectively. Here, k is the Boltzmann constant, T is the absolute temperature in Kelvin, R_L is the load resistance, Δf is the noise equivalent bandwidth of the photodetector and q is the electronic charge.

As mentioned earlier, in a coherent receiver, an optical local oscillator (OLO) signal is added to the received optical signal, and then the resulting optical signal is directed towards a photodetector device. For convenience of discussion, the resultant shot noise is divided into two independent parts: (i) *information signal-dependent* shot noise resulting from the incoming information-bearing optical signal, and (ii) *OLO-dependent* shot noise proportional to the OLO optical power (typically fixed). It turns out that the average power of the information signal-dependent shot noise (of the photocurrent induced) is proportional to the product of the OLO optical power times the received optical signal power [37]. By ensuring a large fixed OLO optical power, the OLO-dependent shot noise component can be made dominant while the effects of the thermal noise and information-signal-dependent shot noise can be made relatively insignificant [7], [38]. This, i.e., OLO-induced-shot noise conditions, is in fact considered to be the *de facto* mode of operation of an (ideal) coherent optical receiver.

In an IM-DD optical system, the intensity-modulated optical signal upon reception is fed directly to the front-end photodetector. The consequent photocurrent at the detector output has a composition as follows: photocurrent (electrical) component

²The shot noise, also known as quantum noise, is a consequence of temporal uncertainty of photons arriving at the photodetector input inducing discontinuous nature of conduction by electrons (at the output) distributed randomly in time [36].

with a one-to-one correspondence to the intensity of the incoming optical signal, information signal-dependent shot noise (recall that there is no OLO here), and thermal noise. Depending on the relative strengths of these two noise components, one can readily infer if the IM-DD optical receiver is operating in *shot noise-limited* condition or *thermal noise-limited* condition. For example, in a power-limited system operating at the minimum required power, thermal noise typically dominates over shot noise. In IM-DD optical systems with large received optical powers (typically holds for most of existing IM-DD terrestrial FSO systems), the signal-dependent shot noise component becomes the dominant noise source while the thermal noise component can be neglected.

A short note on the statistical properties of the shot noise: when the number of received photons per symbol period (or per channel use) is insignificant (e.g., inter-satellite and ground-satellite optical communication), a Poisson model is adequate; otherwise, a Gaussian model suffices [39]. The Gaussian approximation is adequate for most terrestrial application systems; for those interested in a rigorous proof of the Gaussian distribution of the high-intensity shot noise, refer [39], [40].

B. Detection Schemes

In this subsection, we will develop received signal models in the IM-DD and synchronous HD schemes.

Let $x_{\text{IMDD}} \in \mathbb{R}^+$ and $x_{\text{HD}} \in \mathbb{C}$ denote the transmitted signals for the IM-DD and coherent HD systems respectively. In both schemes, the laser source at the transmitter side is constrained by a fixed average (optical) power per symbol constraint as $\mathbb{E}[x_{\text{IMDD}}] \leq P_{\text{avg}}$ and $\mathbb{E}[|x_{\text{HD}}|^2] \leq P_{\text{avg}}$. We remind the reader that the baseband (information) signal in a coherent HD scheme represents a complex optical field, whereas the baseband signal in an IM-DD scheme represents optical intensity. Hence, the optical power constraint in the IM-DD scheme and HD scheme is on the expected value of the signal x_{IMDD} and on the magnitude-squared signal component $|x_{\text{HD}}|^2$ respectively. Adhering to this understanding, the received signal models for the two detection systems are developed next.

1) *Signal-Dependent IM-DD Channel:* The baseband channel (post photodetection) in an IM-DD system is given as

$$y_{\text{IMDD}} := Ix_{\text{IMDD}} + \sqrt{Ix_{\text{IMDD}}}n_s + z_T \quad (11)$$

where y_{IMDD} is the received signal, x_{IMDD} being the transmitted signal, I is the intensity fluctuation due to atmospheric turbulence and misalignment, $z_T \sim \mathcal{N}(0, \sigma_T^2)$ is the signal-independent additive white Gaussian (AWGN) thermal noise, and the scaled component $\sqrt{Ix_{\text{IMDD}}}n_s \sim \mathcal{N}(0, Ix_{\text{IMDD}}\sigma_s^2)$ is the signal-dependent AWGN shot noise [28]. Here, $\sqrt{Ix_{\text{IMDD}}}$ is the scaling term introduced to make the noise variance proportional to the intensity of the received optical signal. As mentioned earlier, the Poisson distribution approximation with a Gaussian distribution is the reason for the formation of Gaussian signal-dependent shot noise.

Remark 4. *In the thermal noise-limited IM-DD channel, $z_T \gg \sqrt{Ix_{\text{IMDD}}}n_s$, i.e., thermal noise is much stronger than the signal-dependent shot noise. The received SNR is given by $|Ix_{\text{IMDD}}|^2/\sigma_T^2$; i.e., the SNR varies as the 'square' of the received optical power.*

In this work, we consider a *shot noise-limited* IM-DD receiver which is typically valid for terrestrial FSO optical operations with large received optical powers. Hence, the total noise variance of the input-dependent IM-DD system (say, σ_{IMDD}^2) is dominated by $I x_{\text{IMDD}} \sigma_s^2$ due to relatively negligible thermal noise component. Thus $\sigma_{\text{IMDD}}^2 \approx I x_{\text{IMDD}} \sigma_s^2$. Correspondingly, conditioned on the intensity fluctuation coefficient I , the *instantaneous* received (electrical) SNR is defined as

$$\gamma_{\text{IMDD}} := I x_{\text{IMDD}} / \sigma_s^2. \quad (12)$$

Here, the SNR grows ‘linearly’ with the received optical power.

2) *Coherent (Heterodyne) Detection*: The ‘complex’ base-band channel in a coherent HD system is described by

$$y_{\text{HD}} := h x_{\text{HD}} + n_{\text{HD}} + w_{\text{T}} \quad (13)$$

where $h \in \mathbb{C}$ is the channel state, $x_{\text{HD}} \in \mathbb{C}$ its input, $y_{\text{HD}} \in \mathbb{C}$ its output, $w_{\text{T}} \sim \mathcal{CN}(0, 2\sigma_{\text{T}}^2)$ the complex AWGN thermal noise, and $n_{\text{HD}} \sim \mathcal{CN}(0, \sigma_{\text{OLO}}^2)$ the (OLO-induced) complex AWGN shot noise [12, Ch. 3]. Note that h represents the fluctuation in the received (complex) optical field and hence $I := |h|^2$ is the intensity fluctuation.

We recall that in an ideal coherent detection receiver, the OLO-induced shot noise is the only dominant noise and thus the total noise power (denoted by σ_{HD}^2) can be approximated by σ_{OLO}^2 . That is $\sigma_{\text{HD}}^2 \approx \sigma_{\text{OLO}}^2$. Conditioned on the channel coefficient h representing fluctuation in the optical field (or equivalently conditioned on the intensity fluctuation coefficient I), the instantaneous (electrical) SNR is defined as

$$\gamma_{\text{HD}} := I |x_{\text{HD}}|^2 / \sigma_{\text{OLO}}^2. \quad (14)$$

C. Ergodic Capacity

The transmitted signal x_{IMDD} in the IM-DD scheme, being optical intensity, is non-negative, while the HD scheme suffers from no such limitation and in fact can support two degrees of freedom. Consequently, the well-known Shannon’s AWGN channel capacity is applicable in the HD scheme but not the IM-DD systems (see [27]).

Based on the received SNRs in (12) and (14), i.e. conditioned on intensity fluctuation coefficient I , the capacities of the optical channels (in nats/s/Hz) based on IM-DD and HD schemes satisfy

$$C_{\text{IMDD}} \geq \frac{1}{2} \log \left(1 + \frac{e}{2\pi} \gamma_{\text{IMDD}} \right), \quad (15)$$

$$C_{\text{HD}} = \log(1 + \gamma_{\text{HD}}). \quad (16)$$

In (15), the constant e is the Euler’s constant. The lower bound (15) on the capacity of the signal-dependent IM-DD channel is deduced from a well-known result in [27, Theorem 7] derived for AWGN IM-DD channel under average-power constraint. More critically, the lower bound is shown to converge to the actual capacity at high received optical powers [27, Proposition 8]. As already mentioned, we consider the IM-DD channel with high received optical powers, and hence the lower bound is in fact a very accurate estimate of the actual capacity.

Based on the above observation and the symmetry of the two FSO systems capacity formulae in (15) and (16), an interesting unification of the two channel capacity expressions (for fixed

channel state) into a single one is possible by introducing a generic parameter k as follows:

$$C(\lambda) := \frac{1}{k} \log \left(1 + \frac{\lambda P_k(\lambda)}{N_k} \right) \quad (17)$$

where $k = 1$, $N_1 = \sigma_{\text{OLO}}^2$, $P_1(\lambda) := |x_{\text{HD}}|^2$ for the HD based scheme and for the IM-DD based scheme, we have $k = 2$, $N_2 = \sigma_s^2 \frac{e}{2\pi}$, $P_2(\lambda) := x_{\text{IMDD}}$. Notice that λ can be viewed as channel (intensity) gain and $P_k(\lambda)$ as the transmitted signal intensity. We average over the random channel gain λ to find the overall average capacity.

We will maximize the (average) optical channel capacity by adapting the laser beam power $P_k(\lambda)$ *optimally* at the transmitter according to the stationary and ergodic time-varying channel fluctuations λ . Power control implicitly conveys that both the transmitter and receiver have perfect channel information at all times. The average optical-power constraint mentioned earlier for both the detection schemes gets translated to $\mathbb{E}[P_k(\lambda)] \leq P_{\text{avg}}$.

Definition 5. The *ergodic-capacity* is the maximum average achievable spectral efficiency (in nats/s/Hz), i.e.

$$\bar{C} := \max_{P_k(\lambda)} \frac{1}{k} \mathbb{E} \left[\log \left(1 + \frac{\lambda P_k(\lambda)}{N_k} \right) \right] \quad (18)$$

where the maximization is over the set of all feasible transmit laser beam adaptation schemes satisfying $\mathbb{E}[P_k(\lambda)] \leq P_{\text{avg}}$.

The optimal laser-beam power allocation P_k^* which maximizes (18) is the classical *waterfilling* in time described by

$$\frac{P_k^*(\lambda)}{N_k} = \left(\frac{1}{\mu_k} - \frac{1}{\lambda} \right)^+ \quad (19)$$

with μ_k chosen so that the optical power constraint is satisfied:

$$\mathbb{E} \left[\left(\frac{1}{\mu_k} - \frac{1}{\lambda} \right)^+ \right] = \text{SNR}_k \quad (20)$$

where $\text{SNR}_k := \frac{P_{\text{avg}}}{N_k}$ is the average transmit power normalized by the average noise power and hence, can be viewed as the average signal-to-noise ratio per symbol. Notice that the parameter μ_k also acts as a channel cutoff and hence the ergodic capacity problem in (18) gets simplified to

$$\bar{C} = \frac{1}{k} \int_{\mu_k}^{\infty} \log \left(\frac{\lambda}{\mu_k} \right) f_{\lambda}(\lambda) d\lambda. \quad (21)$$

IV. UNIFIED EXACT & ASYMPTOTIC CAPACITY RESULTS

To compute \bar{C} , we bifurcate the integral in (21) into three parts as follows:

$$\bar{C} = \frac{1}{k} \left[\underbrace{\int_0^{\infty} \log(\lambda) f_{\lambda}(\lambda) d\lambda}_{=I_1} - \underbrace{\int_0^{\mu_k} \log(\lambda) f_{\lambda}(\lambda) d\lambda}_{=I_2} - \underbrace{\int_{\mu_k}^{\infty} \log(\mu_k) f_{\lambda}(\lambda) d\lambda}_{=I_3} \right]. \quad (22)$$

The evaluation of these integrals is more involved as it seeks a set of transformations, integral identities, integration-by-parts approach, etc. The exact expression is eventually synthesized as a trifecta of solutions of these integrals.

A. Exact Capacity With & Without Pointing Errors

We relegate the integral calculus details involved in the evaluation of I_1 , I_2 , and I_3 to Section V, and state the final capacity result as follows:

Theorem 6. *For the GG atmospheric turbulence channel with pointing error and perfect CSI at both ends, the exact unified capacity is given by*

$$\bar{C} = \frac{1}{k} \left[\log \left(\frac{A_0}{ab} \right) + \psi(a) + \psi(b) - (1/\xi^2) - \log(\mu_k) \right. \\ \left. + \frac{\xi^2}{\Gamma(a)\Gamma(b)} G_{3,5}^{3,2} \left(\frac{ab}{A_0} \mu_k \left| \begin{matrix} 1, 1, \xi^2 + 1 \\ \xi^2, a, b, 0, 0 \end{matrix} \right. \right) \right] \quad (23)$$

where μ_k is solved from the optical power constraint: $\int_{\mu_k}^{\infty} (1/\mu_k - 1/\lambda) f_{\lambda}(\lambda) d\lambda = \text{SNR}_k$.

Proof: The proof is given in Section V. ■

As a baseline for comparison, the unified capacity performance of these FSO schemes in the GG atmospheric turbulence channel *but without* pointing error problem deserves consideration of its own as follows.

Theorem 7. *For the GG atmospheric turbulence channel “without” pointing error and perfect CSI at both ends, the exact unified capacity is given by*

$$\bar{C} = \frac{1}{k} \left[\log \left(\frac{1}{ab} \right) + \psi(a) + \psi(b) - \log(\mu_k) \right. \\ \left. + \frac{1}{\Gamma(a)\Gamma(b)} G_{2,4}^{2,2} \left(ab\mu_k \left| \begin{matrix} 1, 1 \\ a, b, 0, 0 \end{matrix} \right. \right) \right] \quad (24)$$

where μ_k is solved from $\int_{\mu_k}^{\infty} (1/\mu_k - 1/\lambda) f_{\lambda}(\lambda) d\lambda = \text{SNR}_k$.

Proof: Following Remark 2, the fading distribution tends to the (pure) GG distribution without pointing error. Allowing these limiting values of ξ and A_0 in (23) along with the identity [29, Eq. (9.31.1)] completes the proof of the theorem. ■

The capacity result (23) provides some insight on the impact of the fading and pointing error parameters on the FSO systems performances (except for the $\log(\mu_k)$ term and the Meijer-G based term; both of these terms converge in the extreme SNR regimes as explained in the following subsection).

B. Low-SNR & High-SNR Asymptotic Expressions

The asymptotic expansions of these exact capacity results merit special attention as they are much more explicit and simple, and provide clear insights into (how) the key parameters of the fading phenomenon (both GG fading and pointing error) that determine the performance of these FSO schemes.

Theorem 8. *For the GG atmospheric turbulence channel ‘with pointing error’, the asymptotic capacities at low and high SNR are given by*

$$\bar{C}_{low} \approx \frac{1}{k} \left[\frac{A_0}{4ab} \text{SNR}_k \log^2 \left(\frac{1}{\text{SNR}_k} \right) \right], \quad \text{and} \quad (25)$$

$$\bar{C}_{high} \approx \frac{1}{k} \left[\log \text{SNR}_k + \log \left(\frac{A_0}{ab} \right) + \psi(a) + \psi(b) - \frac{1}{\xi^2} \right] \quad (26)$$

where the subscripts ‘low’ and ‘high’ stand for the low-SNR (asymptotically 0) and high-SNR (asymptotically ∞) regimes respectively.

Proof: The proofs require a bit of calculus involving a few low-order series expansions of i) the capacity formula given in Theorem 6 and ii) the average power constraint (20) at low and high SNRs. We delegate these details to Section VI. ■

In [20], the authors have analyzed the capacity performance of this channel but with the *small* pointing error ($\xi^2 \gg 1$) assumption and without dynamic laser-beam power allocation at the optical transmitter side. It happens that the high-SNR capacity asymptote in [20, Eq. (24)] matches exactly with the asymptote obtained in (26), which is understandable as power control becomes less consequential in the high SNR regime. But here, notice that the asymptotic result (26) is in general valid with no constraint on the amount of pointing error displacement (jitter) present at the optical receiver side.

Corollary 9. *For the GG atmospheric turbulence channel ‘without pointing error’, the asymptotic capacities at low and high SNR are given by*

$$\bar{C}_{low} \approx \frac{1}{k} \left[\frac{1}{4ab} \text{SNR}_k \log^2 \left(\frac{1}{\text{SNR}_k} \right) \right], \quad \text{and} \quad (27)$$

$$\bar{C}_{high} \approx \frac{1}{k} \left[\log \text{SNR}_k + \log \left(\frac{1}{ab} \right) + \psi(a) + \psi(b) \right]. \quad (28)$$

Proof: This corollary follows directly from Theorem 8 for the parameters $A_0 \rightarrow 1$ and $\xi \rightarrow \infty$ choice valid for GG distribution without pointing error. ■

The comparison between the high SNR capacity expansions in (26) and (28) provides a measure of the capacity degradation due to pointing errors as summarized below.

Corollary 10. *At high SNR, the capacity loss due to ‘pointing error’ is given by*

$$\frac{1}{k} \left[\frac{1}{\xi^2} - \log(A_0) \right]. \quad (29)$$

Proof: This corollary follows directly by subtracting (26) from (28). ■

The capacity loss due to pointing error in the low-SNR regime can be accounted for using a scaling factor as follows:

Corollary 11. *For the GG turbulence channel, the capacity at low SNRs is scaled by A_0 in the presence of pointing errors.*

Remark 12. *Notice that the input-dependent IM-DD system model is valid only under high transmit/receive power conditions. For this reason, the low-SNR asymptotic results in Theorem 8 and 9 are applicable for the HD scheme only.*

C. Numerical Results: Important Considerations, Comparisons & Discussion

In this subsection, our main focus is on highlighting the analytical utilities of the derived capacity formulae (both exact and asymptotic) further with the help of numerical plots. In several earlier studies on the closely related topics [19], [20], [21], [23] and [24], it is suggested both directly and indirectly that a wide

range of atmospheric turbulence conditions is achievable by varying the FSO channel length. Unfortunately, link length variation also impacts large-scale path loss. The situation becomes more complicated by the fact that the laser beam width expands with propagation distance, which in turn affects the pointing error distribution parameters ξ and A_0 . However, none of these earlier studies have accurately accounted for these intricacies woven together and rather ignored these inter-relations. Although the approach taken seems less reasonable, it does not become a critical factor unless the objective is to isolate and analyze the effect of varying strength of optical turbulence on the FSO systems performance, which is the focal point of research in this paper.

To ensure a fair comparison of the two FSO detection schemes and to provide meaningful insights into the impact of varying atmospheric turbulence conditions with/without pointing error, the FSO Tx-Rx system parameters are maintained constant (optical wavelength, beam-waist at the transmitter, receiver aperture, etc.). Equally important, a horizontal-path terrestrial FSO link of fixed length is considered, keeping the path loss factor ‘unchanged’ which is assumed unity for simplicity. Table I shows the adopted Tx-Rx system settings typical in many practical terrestrial FSO communication systems [9], [10].

TABLE I: FSO SYSTEM & CHANNEL SETTINGS

Parameter	Symbol	Value
Optical wavelength	λ_w	1550 nm
Beam waist (at Tx.)	w_0	1.2 cm
FSO channel length	L	1800 m
Rx. Aperature radius	r_A	1.5 cm
Tx./Rx. optics efficiency	–	100% (assumed)
Path loss factor	–	Unity (assumed)

<i>Gamma-Gamma (GG) fading Parameters</i>		
Turbulence strength	Rytov variance σ_R^2	Gamma-Gamma distribution parameters
Weak	0.8	$a = 4.7424, b = 3.0133$
Moderate	2	$a = 3.9929, b = 1.7018$
Strong	6	$a = 4.8184, b = 1.1896$

<i>GG fading with pointing error Parameters</i> Jitter std. deviation $\sigma_e = 0.1$ m (fixed)			
Turbulence strength	Rytov variance σ_R^2	Pointing jitter parameters	
		ξ	A_0
Weak	0.8	0.4790	0.0490
Moderate	2	0.6302	0.0283
Strong	6	1.0269	0.0107

But how do we achieve variation in the atmospheric turbulence conditions of the FSO channel without affecting the path loss? To this end, we recall that the atmospheric turbulence strength is dictated by $\sigma_R^2 = 1.23 C_n^2 k_w^{7/6} L^{11/6}$ which clearly underscores its dependence on the index of refraction structure parameter C_n^2 (besides, of course, the optical wavelength λ_w and the optical link length L which are assumed fixed in the considered FSO systems and the optical channel setup). In the above-mentioned FSO chan-

nel setting, C_n^2 emerges as the critical parameter characterizing the strength of the atmospheric turbulence as remarked below:

Remark 13. *For a near-ground horizontal propagation path, the index-of-refraction structure parameter C_n^2 remains unchanged and varies with height above ground [9, Section 12.2]. A wide range of optical turbulence conditions is achievable at different altitudes (denoted by h) through $C_n^2(h)$; strong near ground level whereas weak at high altitudes [32, Ch. 2].*

Before proceeding with the numerical results, it is also important to note a key fundamental difference between the two FSO wireless systems, namely IM-DD and HD-based communication systems, that they have very different amount of noise power levels as discussed in the introduction section. The noise level in the direct detection (DD) receiver is generally very large due to the usage of optical filters (typically wideband) for signal or channel selection while the HD detection receiver employs sharp RF filters (with a lower noise level relatively) [7]. For simplicity and concreteness, we assume that the noise power levels (per Hz) in both detection receivers are the same, i.e., $N_1 = N_2 = N_0$, say.

Remark 14. *Notice that $\text{SNR} := P_{\text{avg}}/N_0$ is the average transmit SNR in all the derived capacity formulae (with subscript k now suppressed from the SNR symbol in these capacity formulae as the noise levels are same) and also note that the horizontal axis in Figures 2–9 is the transmit SNR in log scale, not the received SNR. This is done to ensure a fair comparison between the two FSO detection schemes as well as to present a correct numerical analysis of the impact of varying atmospheric turbulence conditions and/or pointing errors. Note that in all the figures to follow, we plot capacity values (bits/sec/Hz is the unit of measurement) by multiplying the derived capacity formulae by $1/(\log 2)$.*

If required, the average received SNR can be computed by scaling the transmit SNR by the mean optical channel gain (denoted by $\mathbb{E}[\lambda]$).

1) *Exact capacity behavior:* Using Theorems 6 and 7, the exact capacities of the HD and IM-DD based optical channels under GG turbulence without and with pointing errors are computed and plotted in Figures 2 and 3 respectively. These values are in excellent agreement with the values obtained by evaluating the original capacity integral (17) numerically for varying atmospheric turbulence levels over a wide SNR range displayed in these figures. Two interesting observations can be drawn from the Figures 2 and 3:

- In the presence of pointing error, there is a sharp decline in the channel capacity performance at high SNRs as can be seen most clearly by comparing Fig. 2 and Fig. 3; a quick intuitive justification for this observation is that the received SNR gets scaled down by the factor $A_0 \xi^2 / (1 + \xi^2)$ due to pointing error.
- Fig. 2 shows the capacity degradation with turbulence at high SNRs for both the detection schemes. The higher the turbulence strength, the greater the loss in capacity; this is expected and can be easily explained by noticing that the probability distribution of the channel gains (especially low gains) is severed with increasing turbulence conditions (refer Fig. 1). Whereas the opposite happens in the presence of pointing error as shown in Fig. 3: for a given pointing error, channel capacity

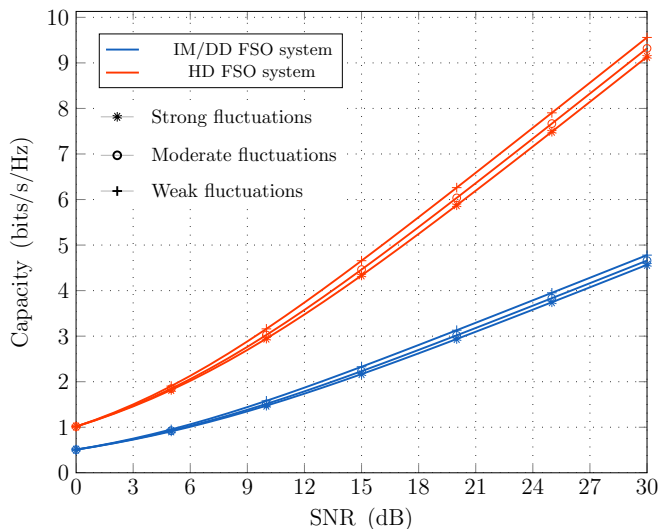


Fig. 2: Capacity results for Gamma-Gamma turbulence channel without pointing error under HD and input-dependent IM-DD detection schemes. The average received SNR is the same as the transmit SNR since the average channel gain $\mathbb{E}[\lambda] = 1$.

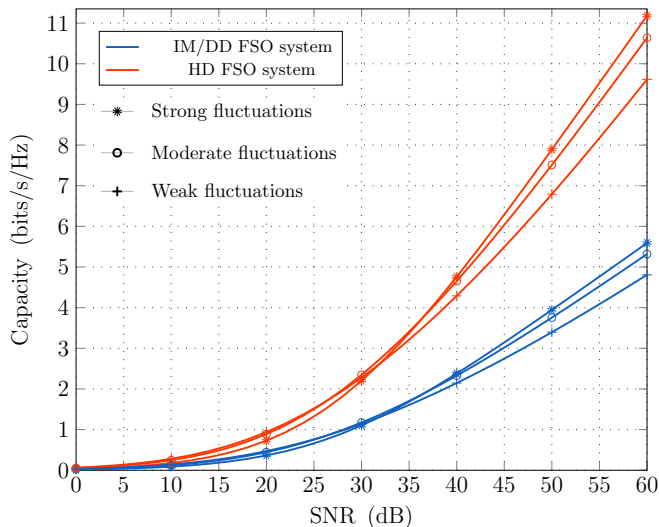


Fig. 3: Capacity results for Gamma-Gamma turbulence channel with pointing jitter under HD and input-dependent IM-DD detection schemes. The (actual) average received SNR is lower than the transmit SNR by the factor $\mathbb{E}[\lambda] = A_0 \xi^2 / (1 + \xi^2)$ (see Remark 1). For example, for strong turbulence condition in Table I, the factor $A_0 \xi^2 / (1 + \xi^2) \approx -22.6$ (dB).

improves at high SNR for stronger turbulence conditions which is very surprising. The explanation to this unexpected capacity behavior is a bit involved. So, we next resort to analyzing the asymptotic behavior in the high SNR regime.

2) *High SNR capacity behavior:* The asymptotic capacity behavior at high SNRs described by (26) in Theorem 8 suggests a comparison with the channel capacity without any turbulence and pointing error, which is the well-known AWGN channel capacity log SNR (at high SNRs). This difference, overall being negative-

valued, can be viewed as ‘capacity penalty’ at high SNRs due to the combined effect of Gamma-Gamma fading and pointing jitter, i.e.,

$$C_{\text{penalty}} \triangleq \log \left(\frac{A_0}{ab} \right) + \psi(a) + \psi(b) - \frac{1}{\xi^2}. \quad (30)$$

Fig. 4 plots the capacity penalty (30) (red curve) as a function of the strength of the atmospheric turbulence. Recall that we have considered a fixed-length horizontal FSO link with a collimated laser beam at the transmitter with the beam waist of $w_0 = 1.2$ cm (see Table I). The beam footprint at the receiver (after propagating over 1.8 km) is expanded due to atmospheric turbulence conditions.

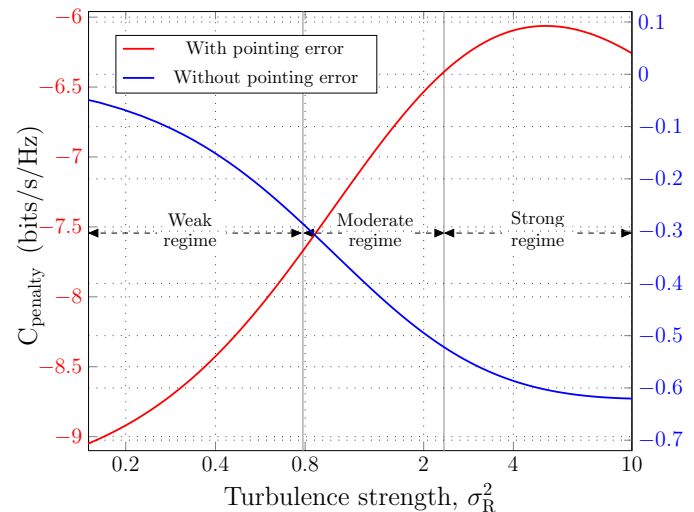


Fig. 4: Capacity penalty at high SNR as a function of turbulence strength for the Gamma-Gamma turbulence channel with and without pointing jitter under HD detection scheme.

This enlarged beam size has two effects:

- it reduces the fraction of the power collected at the fixed-aperture receiver (i.e., A_0 reduces), and
- it reduces the impact of the pointing jitter effect at the receiver (i.e., ξ increases).

The beam enlargement due to greater turbulence yields an increase in capacity at high SNRs because the reduction in the pointing jitter effect more than compensates for the loss in collected power at the receiver, as shown in Fig. 4 for $\sigma_R^2 \leq 6$. Eventually, for very strong turbulence conditions, the pointing jitter effect becomes negligible while the loss in collected power continues leading to capacity loss, as shown in Fig. 4 for $\sigma_R^2 > 6$. We also notice from Fig. 4 that this penalty (at high SNRs) for different turbulence conditions can vary by a large amount (approximately -13 to -8.5 bits/s/Hz).

Whereas in the Gamma-Gamma fading without pointing error, the penalty at high SNRs is described by (see (28))

$$C_{\text{penalty}} = \psi(a) + \psi(b) - \log(ab) \quad (31)$$

and is plotted as blue curve in Fig. 4. Here, the penalty is monotonically increasing with turbulence (refer to the discussion on Fig. 2) and the extent of the penalty is relatively small (approximately -0.9 to -0.1 bits/s/Hz) in comparison with the penalty associated with both fading and pointing error.

Remark 15. The penalty curve (red) in Fig. 4 is valid only for the considered FSO system and turbulence channel settings described in Table I. Keeping the FSO system parameters the same, a similar capacity penalty effect follows for other FSO link lengths; more penalty for shorter link lengths in weak turbulence conditions and vice-versa.

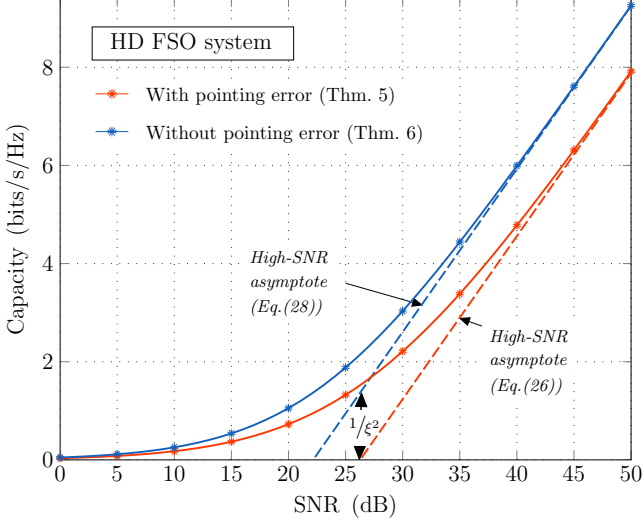


Fig. 5: Capacity results for ‘Strong’ Gamma-Gamma turbulence channels with and without pointing jitter under HD detection schemes (for fading parameters, see the third row in Table I). Note that $A_0 = 0.0107$ is maintained for both exact and asymptotic results (see Remark 16) in both fading channels with and without pointing error.

Remark 16. In almost all the existing related works, the parameter A_0 is neglected for optical fading without pointing error which is quite inaccurate; A_0 can in fact be a small fraction for a fading channel without pointing jitter problem. For an accurate comparison, it is important to consider the impact of A_0 in both with and without pointing error cases, as illustrated in Fig. 5.

In the ‘fixed-length’ optical channel with a fixed FSO system setting as we have considered, it is also possible to estimate the impact of increasing pointing jitter. Recall that σ_e is the pointing jitter’s standard deviation. The loss in capacity (in nats/s/Hz) at high SNRs due to an increase in jitter (only) can be easily deduced from (26) and is given by

$$C_{\text{loss}} \approx \frac{1}{k} \left[\frac{1}{\xi_{\text{new}}^2} - \frac{1}{\xi_{\text{old}}^2} \right] \quad (32)$$

$$= \frac{4(\sigma_{e,\text{new}}^2 - \sigma_{e,\text{old}}^2)}{kw_{L_{\text{eq}}}^2}. \quad (33)$$

where $w_{L_{\text{eq}}}$ is the (fixed) received equivalent beam waist. This is numerically illustrated in Fig. 6.

3) *Low SNR capacity behavior:* As described in the introduction, it is practically interesting to understand the spectral efficiency of terrestrial FSO links operating in the low power regime. The power control aspect of the transmitted laser beam becomes

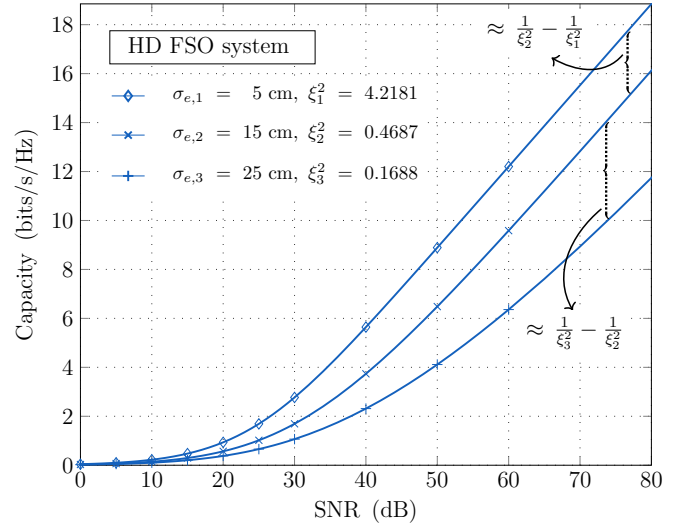


Fig. 6: Capacity of ‘Strong’ Gamma-Gamma turbulence channel under HD detection scheme for varying levels of pointing jitter’s standard deviation σ_e (or ξ^2 equivalently).

important at low-power budgets which necessitates exploiting the channel fading efficiently.

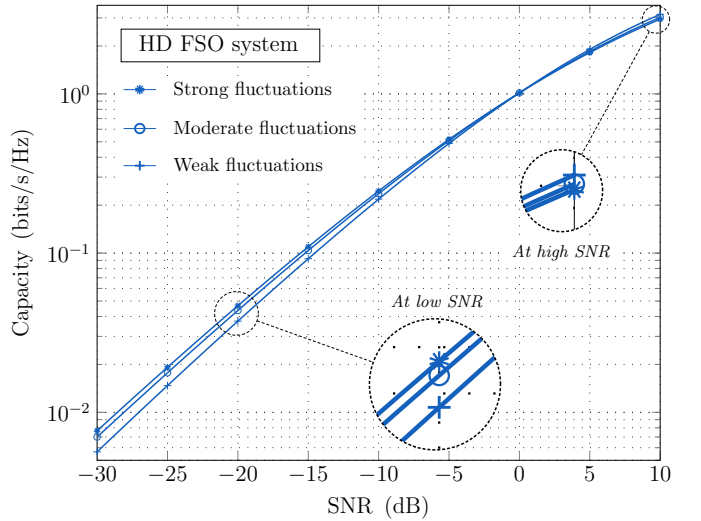


Fig. 7: Capacity results in the low SNR regime for the Gamma-Gamma turbulence channel ‘without’ pointing jitter under HD detection scheme (see Table I for channel turbulence settings). Notice the capacity improvement with turbulence at low SNRs.

Fig. 7 plots the exact capacity for the GG fading channel without pointing error under the HD detection scheme in the low SNR regime. Somewhat surprisingly, the low-SNR capacity is showing improvement with increasing turbulence. This characteristic can also be confirmed from the low-SNR asymptotic expression (27) in Theorem 9; specifically, increasing GG turbulence conditions, say from turbulence profile (a_i, b_i) to the new (a_j, b_j) , yields

$$\text{Capacity improvement factor} \approx \frac{a_j b_j}{a_i b_i}. \quad (34)$$

This improvement in the spectral efficiency can be completely justified by noting that the probability distribution of the higher channel gains improves with turbulence as shown in Fig. 8, which is exploited by the transmitter operating at low SNR (with full CSI) with optical beam power control in an optimized manner. More precisely, the improved probability mass in the tail of the channel gain distribution with atmospheric turbulence suggests that the optical transmitter observes higher channel gains more often under higher turbulence conditions. The optical transmitter allocates beam power for larger channel gains while no power is used for weaker channel coefficients, resulting in an overall improvement in spectral efficiency.

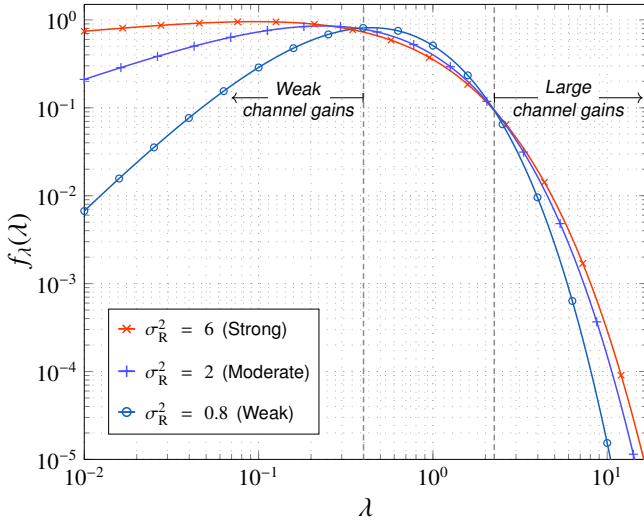


Fig. 8: The PDF of the Gamma-Gamma atmospheric fading gain for the strong, moderate and weak atmospheric turbulence channel settings described in Table I. Notice the increased probability mass for the higher channel gains with increasing atmospheric turbulence. This effect is enhanced in the figure for visual inspection by displaying the fading values on a logarithmic scale.

A similar low-SNR characteristic has been recently reported for the mobile RF single and double-fading channels in [41].

On the other hand, the impact of turbulence on the capacity of the optical channel ‘with’ pointing error at low SNRs becomes more involved. The exact capacity behavior at low SNRs is plotted in Fig. 9 for a wide range of turbulence conditions: the capacity at low SNRs first shows a slight improvement in the weak turbulence regime, but then subsequently deteriorates over the moderate-to-strong turbulence regime.

This peculiar characteristic can be explained using the asymptotic low-SNR capacity result (25) in Theorem 8: the overall effect of both atmospheric turbulence and pointing error on the optical channel capacity at very low SNR (but fixed) is summarily captured in the term $A_0/(4ab)$ which is rearranged as:

$$\text{turbulence scaled factor} \triangleq A_0 \times \frac{1}{4ab}. \quad (35)$$

Fig. 10 plots the variation of the scaled factor (35) (red curve) with turbulence, along with the factor $1/4ab$ (blue curve) which is valid for the pure optical turbulence (see (27)). On comparing

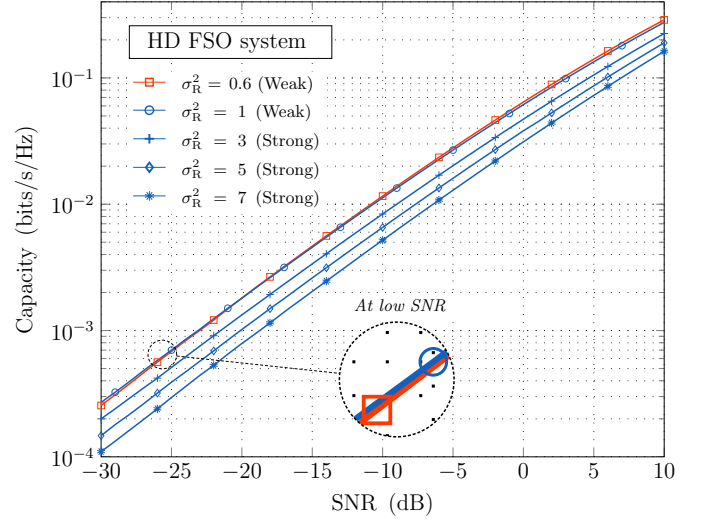


Fig. 9: Capacity results in the low SNR regime for Gamma-Gamma turbulence channel ‘with’ pointing jitter under HD detection scheme.

the two curves, we find that the parameter A_0 (which indicates the fraction of collected power) degrades with turbulence: first slowly in the weak fluctuation regime and then rapidly in strong fluctuation conditions while the factor $1/4ab$ increases. To get some intuition about the variation of A_0 with turbulence, the reader can take a look at the A_0 entries in the Table I described for some typical values of weak, moderate and strong turbulence conditions. Overall, except for weak fluctuations, the channel capacity at sufficiently low SNRs with both fading and pointing error typically degrades with turbulence strength over a wide range of moderate-to-strong conditions; but the opposite is true for the turbulence channel without pointing errors as suggested by the blue curve in Fig. 10 (or refer back to the discussion on Fig. 7).

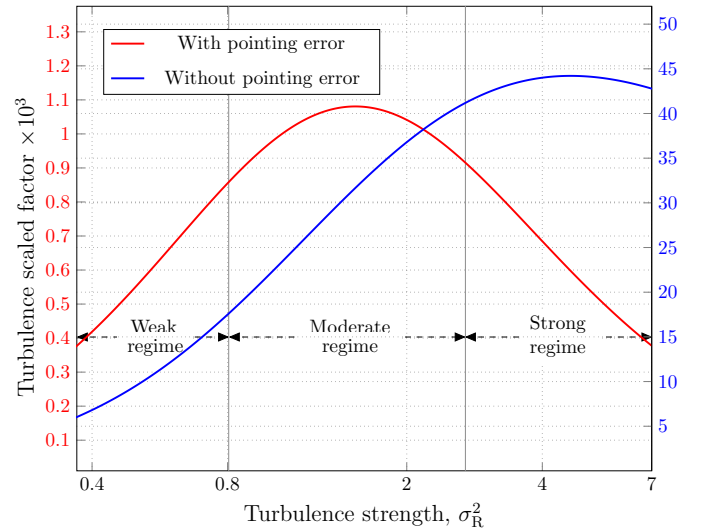


Fig. 10: Variation of the turbulence scaled factor for the GG turbulence channel under HD detection scheme.

V. DERIVATION OF EXACT CAPACITY IN THEOREM 6

The unified capacity expression (from (22)) is summarized as

$$\bar{C} = (I_1 - I_2 - I_3)/k. \quad (36)$$

In the evaluation of the integrals I_1 , I_2 and I_3 , we will repeatedly make use of the following identity [42]:

$$\int x^{j-1} G_{p,q}^{m,n} \left(x \left| \begin{matrix} a_1, \dots, a_p \\ b_1, \dots, b_q \end{matrix} \right. \right) dx = G_{p+1,q+1}^{m,n+1} \left(x \left| \begin{matrix} 1, j+a_1, \dots, j+a_n, j+a_{n+1}, \dots, j+a_p \\ j+b_1, \dots, j+b_m, 0, j+b_{m+1}, \dots, j+b_q \end{matrix} \right. \right). \quad (37)$$

The following subsections describe the calculus details involved in the evaluation of I_1 , I_2 and I_3 .

A. Evaluation of Integral I_1

The integral I_1 can be viewed as

$$I_1 = \mathbb{E} [\log \lambda]. \quad (38)$$

We reformulate (38) by taking expectation on the identity $\frac{d}{dt} \lambda^t = \lambda^t \log(\lambda)$ and thereupon evaluating at $t = 0$ such that

$$\mathbb{E} [\lambda^t \log(\lambda)] \Big|_{t=0} = \frac{d}{dt} (\mathbb{E} [\lambda^t]) \Big|_{t=0}$$

$$\text{and hence } I_1 = \frac{d}{dt} \left(\int_0^\infty \lambda^t f_\lambda(\lambda) d\lambda \right) \Big|_{t=0}. \quad (39)$$

The t -th moment in the RHS of (39) is computed as follows:

$$\int_0^\infty \lambda^t f_\lambda(\lambda) d\lambda = \frac{ab\xi^2}{A_0\Gamma(a)\Gamma(b)} \int_0^\infty \lambda^t G_{1,3}^{3,0} \left(\frac{ab\lambda}{A_0} \left| \begin{matrix} \xi^2 \\ \xi^2 - 1, a - 1, b - 1 \end{matrix} \right. \right) d\lambda. \quad (40)$$

Applying (37) in (40) along with the substitutions that

$$\lim_{x \rightarrow 0} G_{2,4}^{3,1} \left(x \left| \begin{matrix} 1, \xi^2 + t + 1 \\ \xi^2 + t, a + t, b + t, 0 \end{matrix} \right. \right) = 0, \text{ and}$$

$$\lim_{x \rightarrow \infty} G_{2,4}^{3,1} \left(x \left| \begin{matrix} 1, \xi^2 + t + 1 \\ \xi^2 + t, a + t, b + t, 0 \end{matrix} \right. \right) = \frac{\Gamma(a+t)\Gamma(b+t)}{\xi^2 + t},$$

we have

$$I_1 = \frac{\xi^2}{\Gamma(a)\Gamma(b)} \frac{d}{dt} \left(\left(\frac{A_0}{ab} \right)^t \frac{\Gamma(a+t)\Gamma(b+t)}{\xi^2 + t} \right) \Big|_{t=0}. \quad (41)$$

Upon differentiation w.r.t. t and then evaluating the attained expression for $t = 0$, we obtain the final I_1 expression as

$$I_1 = \log \left(\frac{A_0}{ab} \right) + \psi(a) + \psi(b) - \frac{1}{\xi^2}. \quad (42)$$

In the above, we have used $d(\log \Gamma(x))/dx = \psi(x)$, where $\psi(\cdot)$ is the Euler's Digamma function.

B. Evaluation of Integral I_2

In order to compute I_2 , we will first state a simple lemma that gives an (indefinite) integral identity involving the product of the $\log(\cdot)$ and the Meijer-G function.

Lemma 17.

$$\int \log(x) G_{p,q}^{m,n} \left(x \left| \begin{matrix} a_1, \dots, a_p \\ b_1, \dots, b_q \end{matrix} \right. \right) dx = \log(x) \cdot G_{p+1,q+1}^{m,n+1} \left(x \left| \begin{matrix} 1, a_1 + 1, \dots, a_n + 1, a_{n+1} + 1, \dots, a_p + 1 \\ b_1 + 1, \dots, b_m + 1, 0, b_{m+1} + 1, \dots, b_q + 1 \end{matrix} \right. \right) - G_{p+2,q+2}^{m,n+2} \left(x \left| \begin{matrix} 1, 1, a_1 + 1, \dots, a_n + 1, a_{n+1} + 1, \dots, a_p + 1 \\ b_1 + 1, \dots, b_m + 1, 0, 0, b_{m+1} + 1, \dots, b_q + 1 \end{matrix} \right. \right). \quad (43)$$

Proof: Considering the LHS of (43), we apply the integration-by-parts technique treating $\log(\cdot)$ as the first function and the Meijer-G function as the second to get

$$\log(x) \int G_{p,q}^{m,n} \left(x \left| \begin{matrix} a_1, \dots, a_p \\ b_1, \dots, b_q \end{matrix} \right. \right) dx - \int \frac{1}{x} \left(\int G_{p,q}^{m,n} \left(x \left| \begin{matrix} a_1, \dots, a_p \\ b_1, \dots, b_q \end{matrix} \right. \right) dx \right) dx. \quad (44)$$

Applying the identity in (37) transposes (44) to the RHS in (43). This completes the proof. \blacksquare

The integral part I_2 is now evaluated as follows:

$$I_2 = \int_0^{\mu_k} \log(\lambda) f_\lambda(\lambda) d\lambda = \frac{ab\xi^2}{A_0\Gamma(a)\Gamma(b)} \int_0^{\mu_k} \log(\lambda) G_{1,3}^{3,0} \left(\frac{ab\lambda}{A_0} \left| \begin{matrix} \xi^2 \\ \xi^2 - 1, a - 1, b - 1 \end{matrix} \right. \right) d\lambda$$

and using the lemma 17 to get

$$I_2 = \left[G_{2,4}^{3,1} \left(\frac{ab\lambda}{A_0} \left| \begin{matrix} 1, \xi^2 + 1 \\ \xi^2, a, b, 0 \end{matrix} \right. \right) \cdot \log(\lambda) - G_{3,5}^{3,2} \left(\frac{ab\lambda}{A_0} \left| \begin{matrix} 1, 1, \xi^2 + 1 \\ \xi^2, a, b, 0, 0 \end{matrix} \right. \right) \right] \Big|_{\lambda=0}^{\lambda=\mu_k} \frac{\xi^2}{\Gamma(a)\Gamma(b)}. \quad (45)$$

With the following Meijer-G function limits:

$$\lim_{x \rightarrow 0} G_{2,4}^{3,1} \left(x \left| \begin{matrix} 1, \xi^2 + 1 \\ \xi^2, a, b, 0 \end{matrix} \right. \right) \cdot \log(x) = 0, \text{ and}$$

$$\lim_{x \rightarrow 0} G_{3,5}^{3,2} \left(x \left| \begin{matrix} 1, 1, \xi^2 + 1 \\ \xi^2, a, b, 0, 0 \end{matrix} \right. \right) = 0,$$

the final I_2 expression is given by

$$I_2 = \left[G_{2,4}^{3,1} \left(\frac{ab}{A_0} \mu_k \left| \begin{matrix} 1, \xi^2 + 1 \\ \xi^2, a, b, 0 \end{matrix} \right. \right) \cdot \log(\mu_k) - G_{3,5}^{3,2} \left(\frac{ab}{A_0} \mu_k \left| \begin{matrix} 1, 1, \xi^2 + 1 \\ \xi^2, a, b, 0, 0 \end{matrix} \right. \right) \right] \frac{\xi^2}{\Gamma(a)\Gamma(b)}. \quad (46)$$

C. Evaluation of Integral I_3

The I_3 component is given as

$$I_3 = \log(\mu_k) \int_{\mu_k}^\infty f_\lambda(\lambda) d\lambda. \quad (47)$$

where the integral is computed as follows:

$$\begin{aligned} & \int_{\mu_k}^{\infty} f_{\lambda}(\lambda) d\lambda \\ &= 1 - \frac{ab\xi^2}{A_0\Gamma(a)\Gamma(b)} \int_0^{\mu_k} G_{1,3}^{3,0} \left(\frac{ab\lambda}{A_0} \middle| \xi^2 - 1, a - 1, b - 1 \right) d\lambda \\ &= 1 - \frac{\xi^2}{\Gamma(a)\Gamma(b)} G_{2,4}^{3,1} \left(\frac{ab}{A_0} \mu_k \middle| 1, \xi^2 + 1, \xi^2, a, b, 0 \right). \end{aligned} \quad (48)$$

The last equality is obtained by applying the identity in (37) along with the substitution that

$$\lim_{x \rightarrow 0} G_{2,4}^{3,1} \left(x \middle| 1, \xi^2 + 1, \xi^2, a, b, 0 \right) = 0.$$

Substituting these I_1 , I_2 and I_3 expressions back into (36) and consequent simplification gives the final closed-form expression of the capacity as summarized in the Theorem 6.

VI. DERIVATION OF THE ASYMPTOTIC CAPACITY RESULTS IN THEOREM 8

For the purpose of asymptotic capacity analysis, it is useful to derive $\mu_k - \text{SNR}_k$ dependence in the low and high SNR regimes from the average beam power constraint at the optical transmitter.

Lemma 18. *The threshold value μ_k associated with the optimal waterfilling allocation as described in (19) for the transmitted laser beam satisfies*

- 1) $\mu_k \approx \frac{1}{\text{SNR}_k}$ at high SNRs, and
- 2) $\mu_k \approx \frac{A_0}{4ab} \log^2 \left(\frac{1}{\text{SNR}_k} \right)$ at low SNRs.

Proof: Part 1): Substituting (10) into the average optical power constraint (20), we have

$$\frac{\mu_k \text{SNR}_k}{A} = \int_{\mu_k}^{\infty} \left(1 - \frac{\mu_k}{\lambda} \right) G_{1,3}^{3,0} \left(\frac{ab\lambda}{A_0} \middle| \xi^2 - 1, a - 1, b - 1 \right) d\lambda$$

where $A := ab\xi^2/(A_0\Gamma(a)\Gamma(b))$. Applying the identity in (37) to the power constraint equation stated above gives

$$\begin{aligned} \frac{\mu_k \text{SNR}_k}{A} &= \frac{1}{A} - \frac{A_0}{ab} G_{2,4}^{3,1} \left(\frac{ab}{A_0} \mu_k \middle| 1, \xi^2 + 1, \xi^2, a, b, 0 \right) \\ &\quad + \mu_k G_{2,4}^{3,1} \left(\frac{ab}{A_0} \mu_k \middle| \xi^2 - 1, a - 1, b - 1, 0 \right). \end{aligned} \quad (49)$$

We can easily deduce from the power constraint (20) that μ_k bears a strictly monotone and hence one-to-one relation with SNR_k . More precisely, μ_k decreases inversely with increasing SNR_k and vice versa. We particularly note that the contributions from both the Meijer-G functions based terms in (49) for small input argument (due to high SNR values) are vanishingly small and hence

$$\lim_{\mu_k \rightarrow 0} \mu_k \text{SNR}_k = 1.$$

This establishes the $\mu_k - \text{SNR}_k$ relationship described in *Part 1)* for high SNRs.

Part 2): In this part, we seek to obtain an explicit expression for the $\mu_k - \text{SNR}_k$ dependence in the low-SNR regime. As indicated above, the channel cutoff μ_k increases as SNR_k decreases and

hence, the optical transmitter allocates power *only* for very high channel gains at low SNRs. First, we approximate the distribution function of the channel gain $f_{\lambda}(\lambda)$ in (10) using the low-order series expansion of the Meijer's G function for large input arguments provided below:

$$G_{1,3}^{3,0} \left(z \middle| \xi^2 - 1, a - 1, b - 1 \right) \approx e^{-2\sqrt{z}} \sqrt{\pi} z^{\frac{1}{4}(-7+2a+2b)}. \quad (50)$$

Only the largest term in the series expansion is shown in (50) which is then substituted on the LHS of the average power constraint (20) to yield:

$$\text{SNR}_k \approx K \cdot \left[\frac{I_1(\bar{\mu}_k)}{\bar{\mu}_k} - I_2(\bar{\mu}_k) \right] \quad (51)$$

where $K := (\sqrt{\pi} ab \xi^2)/(A_0 \Gamma(a) \Gamma(b))$ is a positive constant independent of the threshold value, and

$$\begin{cases} I_1(\bar{\mu}_k) := \frac{\Gamma(n+1, 2\sqrt{\bar{\mu}_k})}{2^n} \\ I_2(\bar{\mu}_k) := \frac{4\Gamma(n-1, 2\sqrt{\bar{\mu}_k})}{2^n} \end{cases} \quad (52)$$

where, in turn, $\bar{\mu}_k := ab\mu_k/A_0$ is the scaled threshold value, $n := a + b - \frac{5}{2}$, and the $\Gamma(\cdot, \cdot)$ is the upper incomplete Gamma function whose power series expansion at large input is given below [29]:

$$\Gamma(s, t) \approx t^s e^{-t} \left(\frac{1}{t} + \frac{s-1}{t^2} + o\left(\frac{1}{t}\right)^3 \right). \quad (53)$$

By considering only the first two largest terms in (53), (51) gets simplified to

$$\text{SNR}_k \approx K \cdot \left(\frac{ab}{A_0} \mu_k \right)^{\left(\frac{a+b}{2} - \frac{11}{4} \right)} e^{-2\sqrt{\frac{ab}{A_0} \mu_k}}. \quad (54)$$

Taking the logarithm on both sides of (54) and considering only the most significant term by the relative order of magnitude in the right-hand side above, we obtain

$$\log(\text{SNR}_k) \approx -2\sqrt{\frac{ab}{A_0} \mu_k}. \quad (55)$$

Solving (55) for μ_k , we finally arrive at

$$\mu_k \approx \frac{A_0}{4ab} \log^2 \left(\frac{1}{\text{SNR}_k} \right). \quad (56)$$

This completes the proof of the second part. \blacksquare

A. Low-SNR Asymptotics

The low-order series expansion of the Meijer-G function in (23) for large input argument z (asymptotically ∞) is given by

$$\begin{aligned} G_{3,5}^{3,2} \left(z \middle| 1, 1, \xi^2 + 1, \xi^2, a, b, 0, 0 \right) &\approx e^{-2\sqrt{z}} \sqrt{\pi} z^{\frac{1}{4}(-7+2a+2b)} \\ &\quad + \frac{\Gamma(a)\Gamma(b)}{\xi^2} \left(\log(z) + \frac{1}{\xi^2} - \psi(a) - \psi(b) \right). \end{aligned} \quad (57)$$

Substituting the above series expansion in (23), we observe

$$\bar{c} \approx \frac{1}{k} \cdot \frac{K}{(ab/A_0)} \cdot \left(\frac{ab}{A_0} \mu_k \right)^{\left(\frac{a+b}{2} - \frac{7}{4} \right)} e^{-2\sqrt{\frac{ab}{A_0} \mu_k}}. \quad (58)$$

Comparing (58) and (54), we find that

$$\bar{C} \approx \frac{1}{k} \cdot \mu_k \text{SNR}_k. \quad (59)$$

Finally, substituting μ_k from (56) in (59) completes the proof of the low SNR capacity expansion (25) in Theorem 8.

B. High-SNR Asymptotics

At high SNR, the threshold follows $\mu_k \approx \text{SNR}_k^{-1}$ (from lemma 18) whereas the Meijer's G function becomes insignificant for small input argument (asymptotically 0) as

$$\lim_{z \rightarrow 0} G_{3,5}^{3,2} \left(z \left| \begin{matrix} 1, 1, \xi^2 + 1 \\ \xi^2, a, b, 0, 0 \end{matrix} \right. \right) = 0. \quad (60)$$

With these substitutions in Theorem 6, the asymptotic high SNR capacity expression (26) in Theorem 8 is proved.

VII. CONCLUSION

In this work, we analyzed the spectral-efficiency of the existing terrestrial FSO communication systems over Gamma-Gamma atmospheric turbulence channels with optimal beam power allocation incorporated at the transmitter side. The analysis also detailed the negative impact on the performance due to pointing errors impairments present in FSO links.

The derived capacity formulas are explicit: the impact of the fading and pointing error parameters are accurately identified, especially in the extreme SNR regimes. Most notably, we have shown an interesting interplay between the pointing error parameters A_0 and ξ^2 with the variation in turbulence conditions: as the turbulence increases (from weak conditions), there is a rapid improvement in capacity in the high SNR regime because the reduction in the pointing jitter effect more than compensates for the loss in received power. Whereas for the fading channel without pointing errors, the capacity expectedly degrades with turbulence in the high SNR regime.

We have shown that at low SNR, the optical channel capacity improves with increasing turbulence conditions. This happens due to two reasons: i) the distribution of the higher fading gains improves with turbulence, and ii) that the transmitter exploits higher fading gains more efficiently through beam power control. But with pointing errors, the distribution of higher fading gains degrades severely with turbulence leading to capacity loss at low SNRs. Terrestrial FSO communication at low SNRs can be very appealing from a practical point of view for two reasons: firstly, the limited optical power per hertz constraint especially for future high-bandwidth and long-haul applications, and second that communication in a power-limited regime is more energy-efficient. In this context, the low-SNR characterizations mentioned above become significant.

REFERENCES

- [1] S. Arnon, J. Barry, G. Karagiannidis, R. Schober, and M. Uysal, *Advanced Optical Wireless Communication Systems*. Cambridge, U.K.: Cambridge Univ. Press, 2012.
- [2] Q. Liu, C. Qiao, G. Mitchell, and S. Stanton, "Optical wireless communication networks for first- and last-mile broadband access," *IEEE/OSA J. Opt. Netw.*, vol. 4, no. 12, p. 807–828, 2005.
- [3] D. Cornwell, "Laser communication from the Moon at 622Mb/s," 2014. Available online: <http://spie.org/x107507.xml>. [Accessed on 06-September-2023].
- [4] F. Heine, H. Kämpfner, R. Czichy, R. Meyer, and M. Lutzer, "Optical inter-satellite communication operational," in *Proc. IEEE Military Communications Conference (MILCOM)*, 2010, pp. 1583–1587.
- [5] H. Haan and M. Tausendfreund, "Free-space optical data transmission for military and civil applications: A company report on technical solutions and market investigation," in *2013 15th International Conference on Transparent Optical Networks (ICTON)*. IEEE, 2013, pp. 1–4.
- [6] D. J. Heatley, D. R. Wisely, I. Neild, and P. Cochrane, "Optical wireless: The story so far," *IEEE Commun. Mag.*, vol. 36, no. 12, pp. 72–74, 1998.
- [7] J. R. Barry and E. A. Lee, "Performance of coherent optical receivers," *Proceedings of the IEEE*, vol. 78, no. 8, pp. 1369–1394, 1990.
- [8] L. C. Andrews, R. L. Phillips, and C. Y. Hopen, *Laser Beam Scintillation with Applications*. SPIE Press, Bellingham, Wash., 2001, vol. 99.
- [9] L. C. Andrews and R. L. Phillips, *Laser Beam Propagation Through Random Media: Second Edition*. SPIE Press, Bellingham, Wash., 2005.
- [10] S. Bloom, E. Korevaar, J. Schuster, and H. Willebrand, "Understanding the performance of free-space optics," *Journal of Optical Networking*, vol. 2, no. 6, pp. 178–200, 2003.
- [11] S. Arnon, "Effects of atmospheric turbulence and building sway on optical wireless-communication systems," *Opt. Lett.*, vol. 28, no. 2, pp. 129–131, Jan 2003.
- [12] S. Karp, R. M. Gagliardi, S. E. Moran, and L. B. Stotts, *Optical Channels: Fibers, Clouds, Water, and the Atmosphere*. Springer Science & Business Media, 2013.
- [13] M. Al-Habash, L. C. Andrews, and R. L. Phillips, "Mathematical model for the irradiance probability density function of a laser beam propagating through turbulent media," *Optical Engineering*, vol. 40, no. 8, pp. 1554–1562, 2001.
- [14] A. A. Farid and S. Hranilovic, "Outage capacity optimization for free-space optical links with pointing errors," *Journal of Lightwave Technology*, vol. 25, no. 7, pp. 1702–1710, 2007.
- [15] F. Yang, J. Cheng, and T. A. Tsiftsis, "Free-space optical communication with nonzero boresight pointing errors," *IEEE Transactions on Communications*, vol. 62, no. 2, pp. 713–725, 2014.
- [16] A. Jurado-Navas, J. M. Garrido-Balsells, J. F. Paris, A. Puerta-Notario, and J. Awrejcewicz, "A unifying statistical model for atmospheric optical scintillation," in *Numerical Simulations of Physical and Engineering Processes*. Intech Rijeka, Croatia, 2011, vol. 181, no. 8, pp. 181–205.
- [17] M. A. Kashani, M. Uysal, and M. Kavehrad, "A novel statistical channel model for turbulence-induced fading in free-space optical systems," *Journal of Lightwave Technology*, vol. 33, no. 11, pp. 2303–2312, 2015.
- [18] K. P. Peppas, G. C. Alexandropoulos, E. D. Xenos, and A. Maras, "The fisher–snedecor \mathcal{F} -distribution model for turbulence-induced fading in free-space optical systems," *Journal of Lightwave Technology*, vol. 38, no. 6, pp. 1286–1295, 2020.
- [19] W. Gappmair, "Further results on the capacity of free-space optical channels in turbulent atmosphere," *IET Communications*, vol. 5, no. 9, pp. 1262–1267, 2011.
- [20] I. S. Ansari, F. Yilmaz, and M.-S. Alouini, "Performance analysis of FSO links over unified gamma-gamma turbulence channels," in *IEEE 81st Vehicular Technology Conference (VTC Spring)*, 2015, pp. 1–5.
- [21] I. E. Lee, Z. Ghassemlooy, W. P. Ng, M.-A. Khalighi, and S.-K. Liaw, "Effects of aperture averaging and beam width on a partially coherent Gaussian beam over free-space optical links with turbulence and pointing errors," *Applied Optics*, vol. 55, no. 1, pp. 1–9, 2016.
- [22] H. E. Nistazakis, E. A. Karagianni, A. D. Tsigopoulos, M. E. Fafalios, and G. S. Tombras, "Average capacity of optical wireless communication systems over atmospheric turbulence channels," *Journal of Lightwave Technology*, vol. 27, no. 8, pp. 974–979, 2009.
- [23] H. AlQuwaiee, I. S. Ansari, and M.-S. Alouini, "On the performance of free-space optical communication systems over double generalized gamma channel," *IEEE journal on selected areas in communications*, vol. 33, no. 9, pp. 1829–1840, 2015.
- [24] I. S. Ansari, M.-S. Alouini, and J. Cheng, "Ergodic capacity analysis of free-space optical links with nonzero boresight pointing errors," *IEEE Trans. Wirel. Commun.*, vol. 14, no. 8, pp. 4248–4264, 2015.
- [25] O. S. Badarneh, R. Derbas, F. S. Almeahadi, F. El Bouanani, and S. Muhaidat, "Performance analysis of fso communications over \mathcal{F} turbulence channels with pointing errors," *IEEE Communications Letters*, vol. 25, no. 3, pp. 926–930, 2021.
- [26] Y. M. Shishtar, F. H. Ali, and R. C. Young, "Performance analysis of fso communications over a generalized turbulence fading channel with pointing error," *Transactions on Emerging Telecommunications Technologies*, vol. 35, no. 2, p. e4935, 2024.
- [27] A. Lapidath, S. M. Moser, and M. A. Wigger, "On the capacity of free-space optical intensity channels," *IEEE Transactions on Information Theory*, vol. 55, no. 10, pp. 4449–4461, 2009.

- [28] S. M. Moser, "Capacity results of an optical intensity channel with input-dependent Gaussian noise," *IEEE Transactions on Information Theory*, vol. 58, no. 1, pp. 207–223, 2012.
- [29] I. S. Gradshteyn and I. M. Ryzhik, *Table of Integrals, Series, and Products*, 7th ed. San Diego, CA: Academic Press, Inc., 2007.
- [30] H. Weichel, *Laser Beam Propagation in the Atmosphere*. SPIE Optical Engineering Press, Bellingham, 1990.
- [31] B. E. Saleh and M. C. Teich, *Fundamentals of Photonics*. John Wiley & Sons, Ltd, 2019.
- [32] R. R. Beland, *Propagation through Atmospheric Optical Turbulence*. The Infrared and ElectroOptical Systems Handbook, F. G. Smith, ed. (SPIE Optical Engineering Press, Bellingham, Washington), 1993, vol. 2.
- [33] A. A. Farid and S. Hranilovic, "Outage capacity optimization for free-space optical links with pointing errors," *Journal of Lightwave Technology*, vol. 25, no. 7, pp. 1702–1710, 2007.
- [34] J. C. Ricklin and F. M. Davidson, "Atmospheric turbulence effects on a partially coherent Gaussian beam: implications for free-space laser communication," *J. Opt. Soc. Amer. A, Opt. Image Sci.*, vol. 19, no. 9, pp. 1794–1802, Sept. 2002.
- [35] M. Miao, X.-y. Chen, R. Yin, and J. Yuan, "New results for the pointing errors model in two asymptotic cases," *IEEE Photonics Journal*, vol. 15, no. 3, pp. 1–7, 2023.
- [36] B. Oliver, "Thermal and quantum noise," *Proceedings of the IEEE*, vol. 53, no. 5, pp. 436–454, 1965.
- [37] K. Kikuchi, "Fundamentals of coherent optical fiber communications," *Journal of Lightwave Technology*, vol. 34, no. 1, pp. 157–179, 2015.
- [38] G. P. Agrawal, *Fiber-Optic Communication Systems*, 3rd ed. New York: Wiley, 2002.
- [39] A. Chaaban, Z. Rezeki, and M.-S. Alouini, "On the capacity of intensity-modulation direct-detection Gaussian optical wireless communication channels: A tutorial," *IEEE Communications Surveys & Tutorials*, vol. 24, no. 1, pp. 455–491, 2021.
- [40] E. A. Lee and D. G. Messerschmitt, *Digital Communication*. Springer Science & Business Media, 2012.
- [41] K. Singh, "On the capacity of low-rank dyadic fading channels in the Low-SNR regime." 2023. Available online: <https://arxiv.org/abs/2308.05078>.
- [42] Wolfram Research, Inc., "The Wolfram Functions website." Available: <https://functions.wolfram.com/07.34.21.0002.01>. [Accessed on 29-May-2023].